Received: 4 February 2019 | Revised: 10 July 2019 | Accepted: 30 September 2019

DOI: 10.1002/we.2438

RESEARCH ARTICLE

WILEY

Numerical modeling of the hydraulic blade pitch actuator in a spar-type floating wind turbine considering fault conditions and their effects on global dynamic responses

Seongpil Cho[1,2] | Erin E. Bachynski[1,2] | Amir R. Nejad[1] | Zhen Gao[1,2] | Torgeir Moan[1,2]

[1] Department of Marine Technology, NTNU, Trondheim, Norway

[2] Centre for Autonomous Marine Operations and Systems (AMOS), NTNU, Trondheim, Norway

Correspondence
Seongpil Cho, Department of Marine Technology, NTNU, Trondheim, Norway.
Email: seongpil.cho@ntnu.no

Funding information
Research Council of Norway; Equinor, Grant/Award Number: 40136503

Abstract

This paper deals with numerical modeling of the hydraulic blade pitch actuator and its effect on the dynamic responses of a floating spar-type wind turbine under valve fault conditions. A spar-type floating wind turbine concept is modeled and simulated using an aero-hydro-servo-elastic simulation tool (Simo-Riflex [SR]). Because the blade pitch system has the highest failure rate, a numerical model of the hydraulic blade pitch actuator with/without valve faults is developed and linked to SR to study the effects of faults on global responses of the spar-type floating wind turbine for different faults, fault magnitudes, and environmental conditions. The consequence of valve faults in the pitch actuator is that the blade cannot be pitched to the desired angle, so there may be a delay in the response due to excessive friction and the wrong voltage, or slit lock may cause runaway blade pitch. A short circuit may cause the blade to get stuck at a particular pitch angle. These faults contribute to rotor imbalance, which result in different effects on the turbine structure and the platform motions. The proposed method for combining global and hydraulic actuator models is demonstrated in case studies with stochastic wind and wave conditions and different types of valve faults.

KEYWORDS

blade pitch actuator faults, fault characteristics, floating wind turbine, global dynamic responses, hydraulic pitch actuator

Abbreviations: IEC, International Electrotechnical Commission; M#, number (#) of magnitudes; NEM, normalized expected maximum; NREL, National Renewable Energy Laboratory; NRMS, normalized root mean square; OC3, Offshore Code Comparison Collaboration; TF, time of fault occurrence; VCS, circuit shortage in the valve; VEF, excessive friction in the valve; VSL, slit lock in the valve; VWV, wrong voltage applied in the valve

The peer review history for this article is available at https://publons.com/publon/10.1002/we.2438.

1 | INTRODUCTION

Offshore wind turbines operate in ocean environments with irregular waves and turbulent winds and also experience technical faults during their service life. Faults and failures in the actuators, sensors, and system components can lead to system interruptions. They change the system characteristics, the efficiency of power production, and the operational safety. Significant economic losses are associated with operation and maintenance—up to 30% of the life cycle cost for offshore wind farms.[4,5]

Hydraulic pitching drives are still in the majority in older wind turbines as described in Hau.[6] Statistical data on downtime per failure and failure rates of wind turbine sub-systems have been employed to evaluate the wind turbine reliability.[1-3,7] Using failure statistics for wind turbines in Sweden, Ribrant and Bertling[1] showed that the failures in pitch systems accounted for 27.5% of the total component failures. According to the RELIAWIND report,[2] the pitch system has 21.3% and 23.4% contribution to the total failure rate and downtime, respectively. Carroll et al[3] analyzed the failure rates for the offshore wind turbines and their subassemblies, finding that the hydraulics and pitch systems have the highest failure rates among the system components and account for over 14% of the total failures of wind turbines. NordzeeWind[7] shows that the pitch system accounts for over 20% of the production stops.

According to the mentioned references, it is clear that blade pitch systems contribute to the failure rate and downtime of wind turbines. The blade pitch system is critical for wind turbines to maintain constant power generation in above-rated regions of wind speed while protecting the wind turbine from damage. Faults in the blade pitch sensors and actuators influence the control system and result in imbalanced loads on the rotor, main bearings, and shaft. Imbalanced aerodynamic loads on the rotor also affect the power production and the structural responses of the blades, tower, and support structure.

Detailed dynamic analyses of wind turbines under fault situations are required to identify critical conditions and understand the performance of wind turbines. Studies of the effect of pitch system faults on wind turbine performance, loads, and platform motions in wind turbine components have been conducted for specific fault scenarios. Jiang et al[8] and Chaaban et al[9] examine the structural response of floating wind turbines under various pitch mechanism faults. Bachynski et al[10] show the performance of different types of floating wind turbines under pitch actuator fault, grid loss, and shutdown, using a SR-AeroDyn tool. Etemaddar et al[11] analyzed the fault effects in the pitch system on onshore and offshore wind turbines using the extreme response analysis in short term with the HAWC2. These studies focused on the effect of the blade pitch actuator faults on global dynamic responses of the wind turbine. However, the details of the blade pitch actuator were not modeled.

The blade pitch systems of modern wind turbines are driven by electrical or hydraulic pitch actuators.[12] An electrical pitch system requires gears to adjust the pitch angle with an electric motor. It is able to control the position precisely. The main challenges related to electrical pitch systems are gear wear, high backlash, and low robustness against external disturbances. On the other hand, a hydraulic pitch actuator is controlled by a servo or directional control valve, and gears are unnecessary, thus reducing backlash and preventing wear. Hydraulic systems with a high level of stiffness and appropriate damping are suitable in the case of high aerodynamic loads. In particular, rapid load changes in the blade root due to turbulence and wind gusts are controlled and dampened and not transferred through the mechanical system.[13] In addition, hydraulic pitch actuators have low component sensitivity to environment; for example, temperature spans from −25°C to +55°C does not affect the system's performance. The oil in the system reduces structural vibrations and power peaks/loads and increases the overall reliability of the turbine.[14]

Dynamic modeling of the hydraulic actuator for the blade pitch system (valve, cylinder, pump, and reservoir) has been carried out to observe the behavior of wind turbines due to the large blade deflection[15] and fault conditions.[16,17] In these studies, the input voltage is assumed to be directly proportional to the flow rate constants, and the valve spool position is not considered. However, the response of an actual valve is delayed with respect to the input voltage. Carroll et al[3] show that oil, valve, and sludge issues account for a large portion (37.3%) of the total failure rate of hydraulic pitch systems. Therefore, valve modeling and dynamic analysis are essential when considering valve faults in the blade pitch actuator.

This paper focuses on coupled nonlinear aero-hydro-servo-elastic simulations of spar-type floating wind turbines under valve fault conditions. The main contributions of the present work are (a) the numerical modeling of the hydraulic pitch actuator including valve model and spool position controller and (b) modeling of the pitch actuator faults related to mechanical and electrical failures. The hydraulic pitch actuator model is inserted into the global simulation model to investigate how these faults affect the dynamic responses of a floating wind turbine. The objectives of this paper are as follows:

a. Model a hydraulic pitch actuator including a pump, valves, and hydraulic cylinders.
b. Design a proportional-integral (PI) valve controller to achieve satisfactory performance of blade pitching.
c. Model faults in valves.
d. Conduct numerical simulations under fault conditions in aero-hydro-servo-elastic tools coupled with the modeled blade pitch actuator.
e. Compare the wind turbine performance and dynamic responses, eg, blade root bending moments, platform motions, and tower base bending moments, in fault conditions considering different environmental load cases.

In this paper, Section 2 shows the floating wind turbine model, baseline controller, and the hydraulic blade pitch system. Section 3 includes the fault modeling and scenarios for directional control valves. Section 4 shows the simulation results for wind turbine performance, blade root bending moments, platform motions, and tower base bending moments. Section 5 provides the conclusions.

2 | CASE STUDY MODEL AND METHODOLOGY

2.1 | Floating wind turbine model and fully coupled numerical simulation

A spar-type floating turbine has been modeled as a rotor, tower, nacelle, floater, and mooring lines. The model in this paper is based on the National Renewable Energy Laboratory (NREL) 5-MW offshore wind turbine model[18] supported by a spar buoy floater (OC3-Hywind)[19] and three catenary mooring cables as shown in Figure 1. The NREL 5-MW wind turbine specifications are listed in Table 1. In addition, the OC3-Hywind floater properties are provided in Table 2.

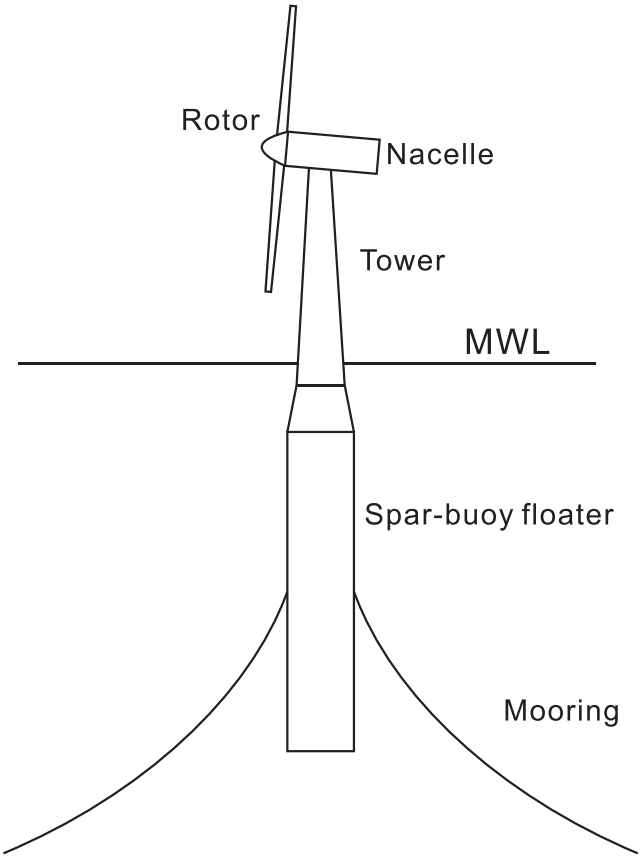

FIGURE 1 Schematic view of a spar-type floating wind turbine

TABLE 1 Properties for the National Renewable Energy Laboratory (NREL) 5-MW wind turbine[18]

Rated power, MW	5
Rotor orientation and configuration	Upwind, three blades, horizontal axis
Rotor diameter, m	126
Hub height from the mean water level, m	90
Cut-in, rated, cut-out wind speed, m/s	3, 11.4, 25
Cut-in, rated rotor speed, °/s	41.4, 72.6
Max pitch rate, °/s	8
Gearbox ratio	97

TABLE 2 Properties for the OC3-Hywind floater[19]

Water depth, m	320
Draft, m	120
Diameter above taper, m	6.5
Diameter below taper, m	9.4
Center of mass, m	(0, 0, −89.9115)
Mass, including ballast, kg	7.466×10^6
Mass moment of inertia (I_{xx} and I_{yy}), kg·m^2	4.229×10^9
Mass moment of inertia (I_{zz}), kg·m^2	1.642×10^8

The dynamic responses of the wind turbine model have been simulated with SR,[20,21] which is an aero-hydro-servo-elastic code for fully coupled nonlinear time-domain numerical simulations. Hydrodynamic forces and moments on the rigid hull, according to first-order potential flow theory and Morison-type viscous drag, have been accounted for in Simo.[20] The flexible elements for the blades, shaft, tower, and mooring system with the finite element solver are modeled in Riflex.[21] Additionally, Riflex calculates the aerodynamic forces and moments on the blades based on the blade element momentum (BEM) method including tower shadow, dynamic stall, and skewed inflow correction.[21] The models for structural dynamics, hydrodynamics, and aerodynamics are considered simultaneously with an external code that consists of (a) a baseline control system for a torque and pitch controller and (b) a model of the blade pitch system under various operational conditions. Figure 2 shows the data transmission of SR and controller algorithm.

2.2 | Baseline controller for operational wind turbines

The baseline control system consists of the blade pitch and generator torque controllers. In the below-rated wind speed region, the torque controller is active to capture the maximum power by regulating the generator torque and thus maintaining the optimal tip speed ratio.[18] In above-rated wind speed region, the blade pitch controller adjusts the blade pitch angle to reduce the aerodynamic loads while producing the rated power. For floating wind turbines, the blade pitch controller may be used to improve the system responses and reduce the floater motions.[22] In the baseline controller[18] developed by NREL, the pitch actuator is not modeled; it is assumed that the blade pitch angle can be adjusted directly the pitch command. In this paper, a hydraulic pitch actuator is modeled and interacts with the baseline controller with modified proportional and integral gain values.[19] Figure 3 shows the block diagram of the modified baseline controller, where Ω_r is the rotor speed, Ω_g is the generator speed, $\Omega_{g,m}$ is the measured generator speed, $\Omega_{g,\text{rated}}$ is the rated generator speed, Q_g is the generator torque, Q_a is the aerodynamic torque, β_m is the measured blade pitch angle, and V_{wind} is the wind speed.

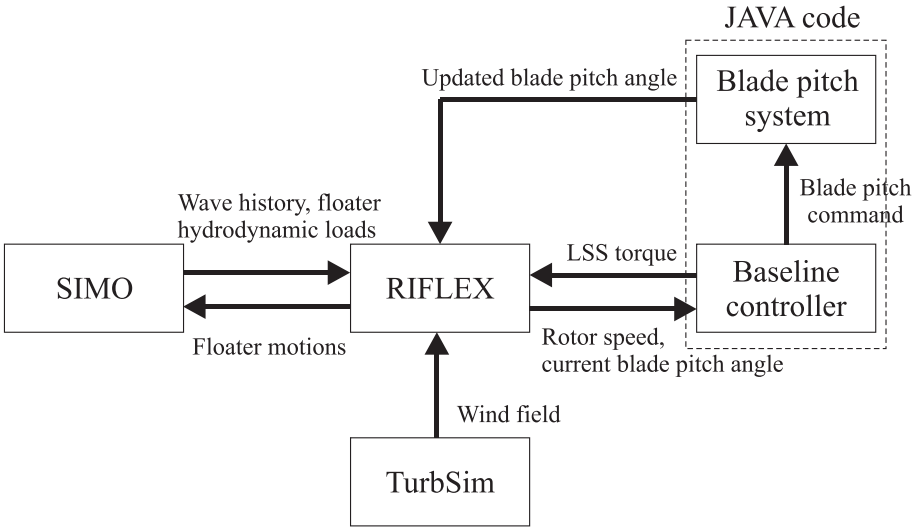

FIGURE 2 Data transmission between Simo-Riflex (SR) and controller

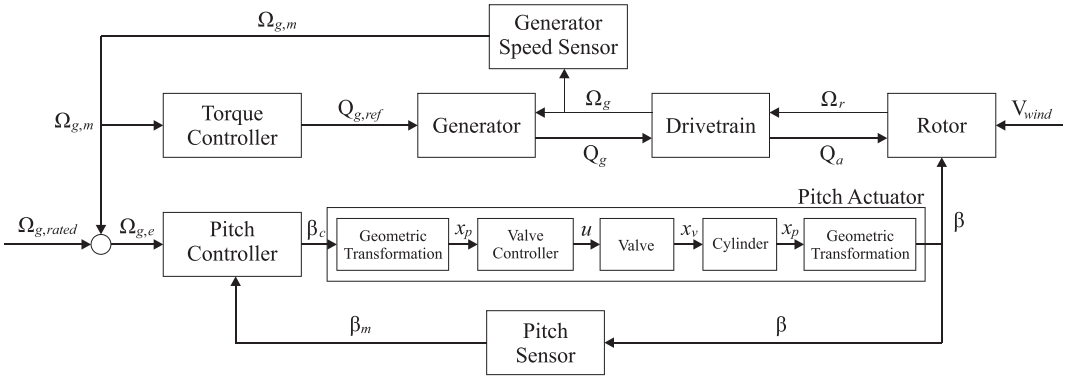

FIGURE 3 Block diagram of the baseline controller

2.3 | Hydraulic actuator system

The hydraulic pitch system includes the hydraulic pump, a set of directional control valves, a fluid tank, and a hydraulic cylinder. The blade pitch angle is controlled by a hydraulic cylinder placed in the hub of the turbine. Hydraulic pitch control is not sensitive to vibrations. The oil flow to and from the cylinders is controlled by a number of valves, in particular a control valve. The energy to drive the hydraulic cylinders is supplied by a power unit placed in the nacelle, and the energy is transferred to the hub via a rotary union.

The system controller provides a command voltage signal to control the valve spool position based on the difference between the blade pitch angle and the reference signals. The schematic diagram of a hydraulic actuator as shown in Figure 4A consists of a constant pressure pump, an accumulator, a reservoir, a hydraulic cylinder, and a directional control valve.

2.3.1 | Directional control valve model

The directional control valve uses an electromagnetic field via the solenoid coil to move an internal steel armature assembly. This assembly controls the position of the main cylinder to change the state of the main valve to open or closed. Figure 5 shows the schematic of a 4/3 directional control valve with solenoid.

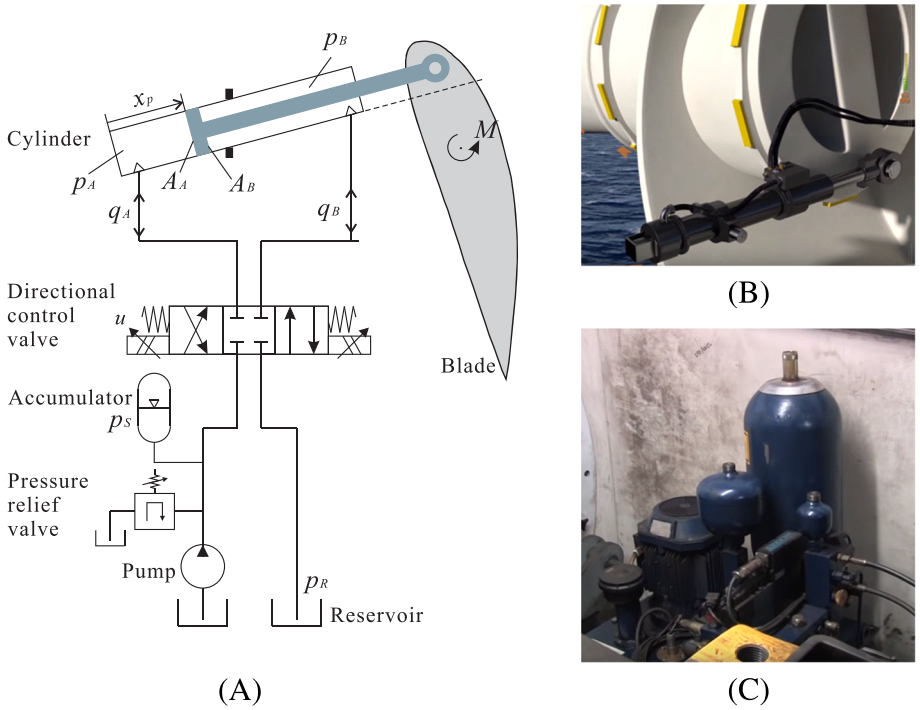

FIGURE 4 The hydraulic pitch system: (A) schematic diagram, (B) hydraulic actuator,[23] and (C) hydraulic power station[24] [Colour figure can be viewed at wileyonlinelibrary.com]

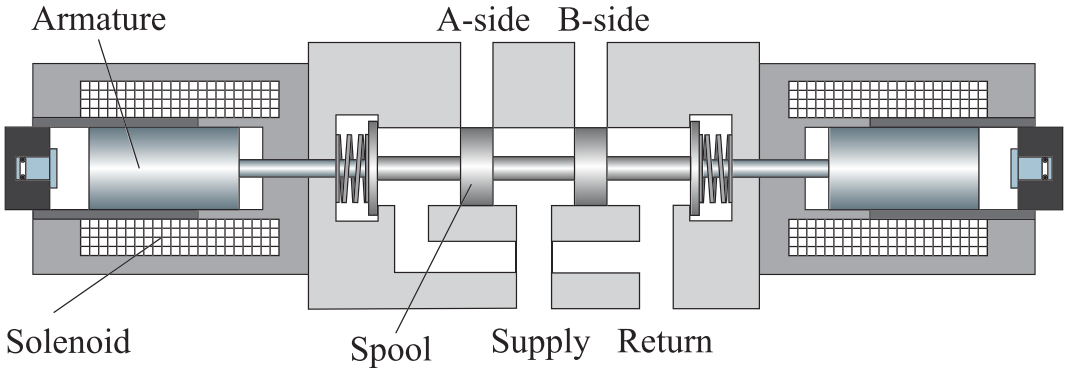

FIGURE 5 4/3 directional control valve with solenoid [Colour figure can be viewed at wileyonlinelibrary.com]

To control the blade pitch angle, the valve spool position control adjusts the hydraulic flow into the cylinder. The valve spool position x_{vs} is calculated from the control input voltage u_{vs} through a second-order system[25] given by

$$\ddot{x}_{vs} + 2\zeta_{vs}\omega_{vs}\dot{x}_{vs} + \omega_{vs}^2 x_{vs} = \omega_{vs}^2 k_u u_{vs}, \tag{1}$$

where ω_{vs} is the valve natural frequency, ζ_{vs} is the valve damping ratio, k_u is the voltage gain, respectively, and $(\dot{})$ represents the time derivatives. It is assumed that the valve spool is symmetric with zero overlap design.

As described in Figure 6, flow directions can be determined by the valve spool position. If the spool is at the right-side position ($x_{vs} > 0$) as shown in Figure 6B, hydraulic fluid flows from the pump (supply) into the cylinder chamber B side and from the cylinder chamber A side to the reservoir tank (return). On the other hand, if the spool position is set to the left-side position ($x_{vs} < 0$) in Figure 6C, then the hydraulic fluid can flow from pump to A side and B side to the reservoir tank. Hydraulic fluid cannot flow when the valve spool is at the neutral position ($x_{vs} = 0$).

The hydraulic flow rate at A and B can be determined based on the spool position. The continuity equation of hydraulic flow rate at A and B depends on the sign of the spool position:

For $x_{vs} > 0$,

$$\begin{aligned} q_A &= -k_q x_{vs}\sqrt{p_A - p_R}, \\ q_B &= k_q x_{vs}\sqrt{p_S - p_B}, \end{aligned} \tag{2a}$$

and for $x_{vs} < 0$,

$$\begin{aligned} q_A &= -k_q x_{vs}\sqrt{p_S - p_A}, \\ q_B &= k_q x_{vs}\sqrt{p_B - p_R}, \end{aligned} \tag{2b}$$

where q_A and q_B are the hydraulic flow rates to the cylinder chamber A and B sides, k_q is the valve flow coefficient, and p_S and p_R are the supply pressure and the return pressure, respectively. Table 3 describes properties for the directional control valve from Rexroth's valve model (RE 29093, size 16).[26] The supply pressure p_S is set to 250 bars controlled by the accumulator.

From Merritt,[27] the valve flow coefficient can be calculated by

$$k_q = \frac{C_d A_d}{x_{vs,\max}}\sqrt{\frac{2}{\rho_{\text{fluid}}}}, \tag{3}$$

where C_d is the discharge coefficient, A_d is the discharge area, and ρ_{fluid} is the density of fluid.

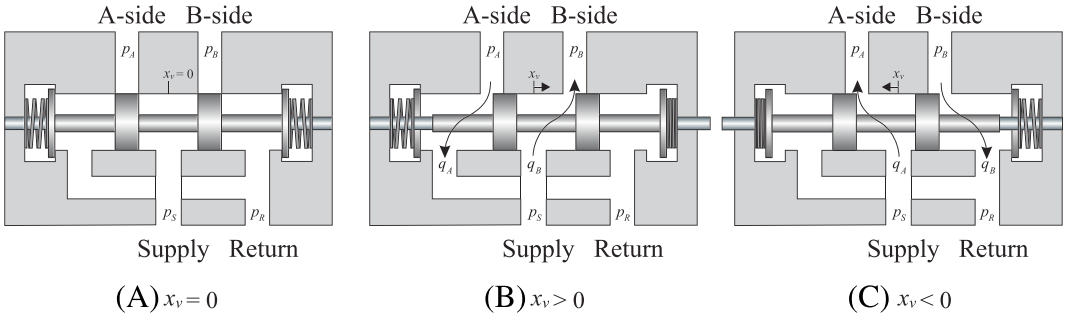

FIGURE 6 Flow mechanism of the valve with spool position [Colour figure can be viewed at wileyonlinelibrary.com]

TABLE 3 Properties for the directional control valve[26]

Valve natural frequency (ω_{vs}), rad/s	141
Valve damping ratio (ζ_{vs})	0.74
Minimum and maximum valve position ($x_{vs,min}$, $x_{vs,max}$), m	−0.02, 0.02
Minimum and maximum input voltage ($u_{vs,min}$, $u_{vs,max}$), V	−10, 10
Valve voltage gain (k_u), m/V	0.002
Valve flow gain (k_q), $m^2/s/\sqrt{bar}$	0.0233

However, it is hard to directly calculate the exact discharge coefficient C_d values from the technical data. Alternatively, k_q values can be estimated by Equation 4 from Albers[28] and Šulc and Jan[29] with the nominal pressure drop (Δp_N) and nominal flow rate (q_N) from Rexroth's valve model.[26]

$$k_q = \frac{q_N}{x_{vs,max}\sqrt{0.5\Delta p_N}} \tag{4}$$

2.3.2 | Blade pitch dynamics

Calculation of hydraulic force in a cylinder

As illustrated in Figure 4, the hydraulic actuator is modeled by a single-rod and double-acting cylinder that consists of a piston inside a cylindrical housing. The cylinder produces the force from hydraulic pressure acting on the piston. The pressure dynamics based on the flow mechanism into two chambers (A and B sides) in the cylinder are written by

$$\dot{p}_A = \frac{E_{\text{eff}}}{V_A(x_p)}(q_A - A_A\dot{x}_p), \tag{5a}$$

$$\dot{p}_B = \frac{E_{\text{eff}}}{V_B(x_p)}(q_B + A_B\dot{x}_p), \tag{5b}$$

where V_A and V_B are the total control volumes of chambers A and B depending on the piston position x_p. A_A and A_B are the areas of the piston on the A and B sides. E_{eff} is the effective bulk modulus of the hydraulic fluid that is assumed to be incompressible. Additionally, the volumes V_A and V_B are calculated by

$$\begin{aligned} V_A(x_p) &= V_{A0} + A_A x_p, \\ V_B(x_p) &= V_{B0} + A_B(l_p - x_p), \end{aligned} \tag{6}$$

where V_{A0} and V_{B0} are the initial volumes of the two-cylinder chamber.

By calculating hydraulic pressures in sides A and B of the cylinder, the piston force F can be obtained as follows:

$$F = P_A A_A - P_B A_B. \tag{7}$$

Blade pitch dynamics

The blade pitch angle can be adjusted by the hydraulic actuator controlled by a pitch moment from piston force F acting on the rigid bar. Figure 7 shows the geometry of the hydraulic pitch actuator. The geometry of the actuator is related to the piston position x_p and the pitch angle β by

$$x_p(\beta) = \sqrt{L_p^2 + r_p^2 - 2L_p r_p \cos(\alpha_0 - \beta)} - l_p/2, \tag{8}$$

where r_p is the torque arm, l_p is the rod length, L_p is the length between the pivot and rotational center, and α_0 is the initial angle between the pin-to-center axis and the torque arm when x_p = 0. From the geometry of this actuator, the blade pitch torque $M_{T,bp}$ can be described by

$$M_{T,bp} = F r_p g(\beta), \tag{9}$$

where the $g(\beta)$ is a force factor represented by $g(\beta) = \dfrac{1}{r_p}\dfrac{dx_p}{d\beta}$.

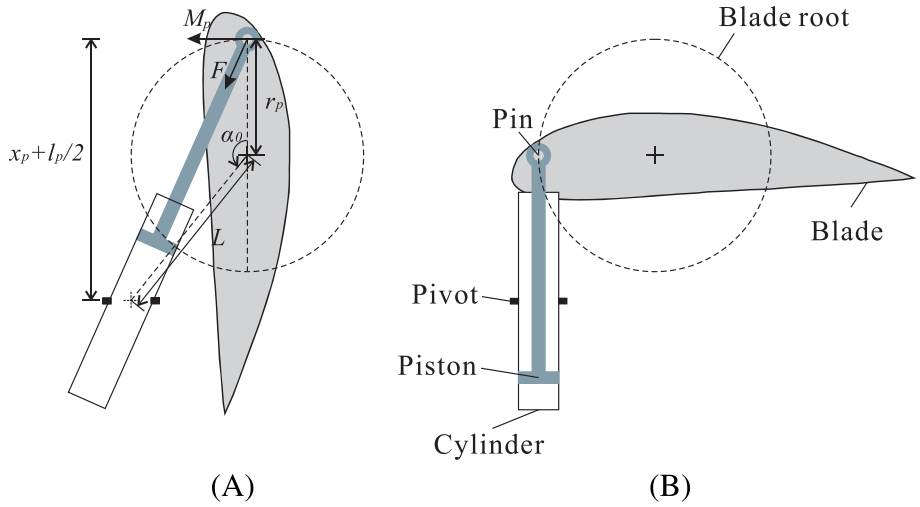

FIGURE 7 Geometry of the blade pitch actuator: (A) β = 0° and (B) β = 90° [Colour figure can be viewed at wileyonlinelibrary.com]

The pitch angle dynamics are governed by

$$J_{bp}\ddot{\beta} + B_{bp}\dot{\beta} = M_{T,bp} + M_A, \tag{10}$$

where J_{bp} is the pitch inertia, B_{bp} is the viscous damping coefficient, and M_A is the aerodynamic pitching moment.

Table 4 shows the pitch actuator geometries and parameters. However, it is hard to directly measure the viscous damping coefficient B_{bp}. Therefore, an alternative method, described in Section 2.4, was used to estimate B_{bp}.

2.4 | Valve spool position control

The blade pitch angle β can be determined by the piston position x_p in the hydraulic cylinder based on the geometrical relationship as described in Equation (8). The piston position x_p of the cylinder is controlled by the valve spool position x_{vs} corresponding to the desired position. The valve spool position is changed according to the input voltage applied to the directional control valve.

First, the control input u_v can be calculated by a PI controller from the piston position error $e(t)$ feedback to the directional control valve position as follows:

$$u_{vs}(t) = k_p\left(e(t) + \frac{1}{T_i}\int_0^t e(\tau)d\tau\right),\ e(t) = (x_p(\beta) - x_p(\beta_C)), \tag{11}$$

where k_p is the proportional gain, T_i is the integral time, and the position error $e(t)$ is given as function of the blade pitch angle β and pitch command β_C from the pitch controller in Figure 3.

In order to calculate the proportional gain k_p, the valve and pitch cylinder systems need to be transformed by transfer function in steady-state condition. The directional control valve model can be described by the transfer function $G_{vs}(s)$ obtained from Equation (1).

TABLE 4 Pitch actuator geometries and parameters[30]

Piston rod length (l_p), m	**2**
Torque arm (r_p), m	1
Pin-to-center axis length (L_p), m	1.7
Initial angle (α_0), rad	2.5128
Pitch inertia (J_{bp}), kg·m^2	28 600
Viscous damping coefficient (B_{bp}), N·s/rad	8.545×10^5
Effective bulk modulus (E_{eff}), bar	18 000

$$G_{vs}(s) = \frac{X_{vs}(s)}{U_{vs}(s)} = \frac{\omega_{vs}^2 k_u}{s^2 + 2\zeta_{vs}\omega_{vs}s + \omega_{vs}^2}, \tag{12}$$

where $U_{vs}(s)$ and $X_{vs}(s)$ are the transfer functions of the valve system input (voltage) and output (valve spool position). The blade pitch system in a steady-state condition can be modeled by third-order transfer function from Merritt.[27] .

$$G_{bp}(s) = \frac{B(s)}{X_{vs}(s)} = \frac{C_p\omega_p^2}{s^3 + 2\zeta_p\omega_p s^2 + \omega_p^2 s}, \tag{13}$$

$$\omega_p = g\sqrt{\frac{E_{eff}}{J_{bp}}\left(\frac{A_A^2}{V_A} + \frac{A_B^2}{V_B}\right)},\ \varsigma_p = \frac{B_{bp}}{2\sqrt{J_{bp}E_{eff}g\left(\frac{A_A^2}{V_A} + \frac{A_B^2}{V_B}\right)}} \tag{14}$$

$$C_p = \frac{\left(\frac{A_A k_q\sqrt{\Delta p_A}}{V_A} + \frac{A_B k_q\sqrt{\Delta p_B}}{V_B}\right)}{g\left(\frac{A_A^2}{V_A} + \frac{A_B^2}{V_B}\right)}, \tag{15}$$

where $X_{vs}(s)$ and $B(s)$ are the transfer functions of the blade pitch system input (valve spool position) and output (blade pitch angle), ω_p is the natural frequency of piston system, ζ_p is the damping ratio, and C_p denotes the flow rate gain. The volume V and force factor g can be changed to influence each natural frequency and damping ratio of the pitch system in steady-state condition. The minimum damping ratio for the system is 0.2 from Merritt.[27] Then, B_{bp} is calculated by Equation (14).

Total system transfer function $G_T(s)$ can be derived by

$$G_T(s) = G_{vs}(s)\,G_{bp}(s) = \frac{B(s)}{U_{vs}(s)} = \frac{\omega_{vs}^2\omega_p^2 k_u C_p}{s\left(s^2 + 2\zeta_{vs}\omega_{vs}s + \omega_{vs}^2\right)\left(s^2 + 2\zeta_p\omega_p s + \omega_p^2\right)}. \tag{16}$$

To set the critical proportional gain $k_{p,\text{crit}}$, the characteristic equation and Routh's methods were applied. Stability should be checked in every piston position in cylinder for the pitch angles from 0° to 90°. Using an empirical method and applying $k_{p,\text{crit}}$ values from 1 to 300 in the system, the critical proportional gain is found to be $k_{p,\text{crit}}$ = 139.2 V/rad in every piston position and pitch angle. The period of oscillation T_c = 0.3012 second can be calculated by applying $k_{p,\text{crit}}$ and Routh's methods as described in Dutton et al. [31] Using the Ziegler-Nichols method,[31] the proportional gain and integral time are therefore set to $k_p = 0.45k_{p,\text{crit}}$ and $T_i = T_c/1.2$ in case of PI control, respectively. The blade pitch control system is tested for the 15° step reference signal in Figure 8. The response of the blade pitch angle, valve spool position, and control input voltage shown here demonstrates the ability to follow the pitch angle reference and for controller performance.

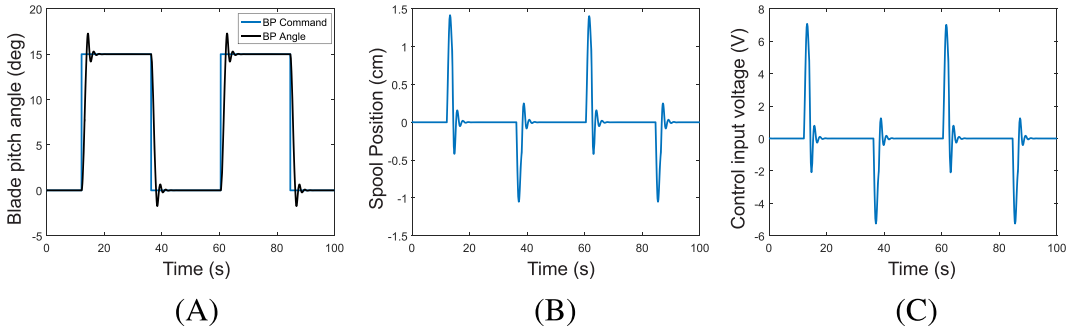

FIGURE 8 The step response of the blade pitch system with 15° step reference signal: (A) blade pitch angle, (B) valve spool position, and (C) control input voltage [Colour figure can be viewed at wileyonlinelibrary.com]

3 | FAULT MODELING AND SCENARIOS

Carroll et al[3] show that oil, valve, and sludge issues account for a large portion (37.3%) of the total failure rate for hydraulic pitch systems. Valve faults can change the system characteristics.[25]

Basically, faults in the directional control valves are mainly categorized as mechanical or electrical faults. Mechanical faults are related to oil contamination and sludge that disturb the spool movement, acting as increasing friction in the valve. Electrical faults may be related to additional and residual current through the solenoid due to damage or dirt on the armature. After these faults occur, the valve cannot provide an adequate amount of flow in the cylinder from control input. These faults influence the results of pressure, piston force, blade pitch angle, and response delay. They also could affect the global dynamic response of wind turbines in transient and steady-state conditions. The incorrect pitching of a blade due to faults causes asymmetric forces on blades, introducing an unbalanced rotation, which increases structural loads on the rotor significantly. In the worst cases, it is associated with valve seizure that leads to inoperable conditions.

In this paper, four different cases of valve faults are considered (two mechanical faults and two electrical faults): excessive friction (VEF), slit lock (VSL) on spool, wrong voltage applied (VWV), and circuit shortage (VCS), in the directional control valve. Figure 9 illustrates mechanical and electrical valve faults. These faults are selected based on information in Institute of Electrical and Electronics Engineers,[2] Cho et al,[32] and Watton.[33]

3.1 | Mechanical faults

Directional control valves operate over thousands of cycles with adequate oil and undergo mechanical and thermal stresses periodically in a normal operation state. The operational conditions mainly influence the service life of the valve. According to Carroll et al,[3] oil contamination causes up to 25% of the total failures in hydraulic systems. Oil contamination with poor filtration results in sludge buildup on the surface of spool and bore. The sludge is a mixture of rusted metal particles, sand, dust, and polish compound.

As the sludge builds up on the spool, the clearances between the spool and body decrease. This decreased clearance space leads to more force being required to move the spool as the static friction increases. This fault is called excessive friction in valves (VEF). The increasing friction is modeled as follows:

$$\ddot{x}_{vs} + 2\zeta_{vs}\omega_{vs}\dot{x}_{vs} + \omega_{vs}^2 x_{vs} = \omega_{vs}^2 k_u u_{vs} - F_F, \tag{17}$$

$$F_F = F_C \mathrm{sgn}(\dot{x}_{vs}), \tag{18}$$

where F_C is the Coulomb friction. The value of friction F_F in the normal condition is set to 0 because it is negligible in real valve spools.

This sludge narrows the clearance, allowing more particles into the clearance space. In the worst case, these mixtures with sludge buildup and particles become hardened. If the friction is larger than the maximum force from the solenoid, the valve spool will be seized. This phenomenon is commonly referred to as "slit lock." When slit lock (VSL) in valves occurs, the spool position is described by

$$x_{vs} = x_{vs,\mathrm{VSL}}, \tag{19}$$

where $x_{vs,\mathrm{VSL}}$ is the spool position after the VSL fault.

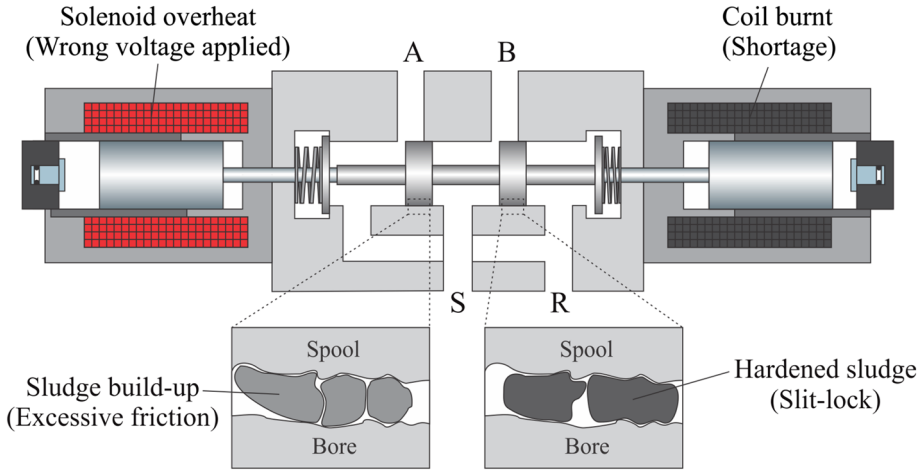

FIGURE 9 Illustration of mechanical and electrical valve faults [Colour figure can be viewed at wileyonlinelibrary.com]

3.2 | Electrical faults

When the solenoid coil reaches the magnetic saturation level, the coil is overheated caused by high inrush currents. This phenomenon changes its coil impedance and the current through the solenoid. In extreme cases, the core of the solenoid is subject to damages, or the coil inductance is permanently changed. Then, it applies the wrong voltage.

The wrong voltage applied (VWV) resulting from changed coil impedance can be described by changing the valve voltage gain k_u,

$$k_u = k_{u,\mathrm{WV}}, \tag{20}$$

where $k_{u,\mathrm{WV}}$ is changed voltage gain.

Furthermore, if solenoids cannot properly dissipate the heat generated by their residual current or go through high inrush current due to faults, then the solenoid is damaged and burnt out, which means that the insulation around the coil windings will burn and the coil will short out. When a solenoid circuit shortage occurs (VCS), the voltage applied is as follows:

$$u_{vs} = u_{\mathrm{VCS}} = 0, \tag{21}$$

where u_{VCS} is the voltage value in the VCS fault. If a VSC fault occurs in the valve system, the spool position reacts and moves to a neutral position that allows no flow due to the spring described in Figure 5. Then, the valve is closed, and the actuator gets stuck in the same position. Table 5 describes the updated fault values in the valve model and consequences in each fault.

4 | SIMULATION RESULTS AND DISCUSSION

In this section, simulation results are presented to illustrate the effect of the valve fault conditions. Numerical simulations are conducted under four different fault cases: VEF, VSL, VWV, and VCS, on a single blade.

4.1 | Environmental conditions

Four load cases with different wind and wave conditions were selected for simulating the dynamic responses of the floating wind turbine, as given in Table 6.

The turbulent wind field $U_w(x, y, z, t)$ represented by the normal wind profile and the normal turbulence model is modeled by using TurbSim[34] according to the Kaimal turbulence model. The wind model was based on the International Electrotechnical Commission (IEC) 61400-1[35] and 3[38]. In the vertical plane, 32 × 32 points were used over an area of 160 × 160 m, with time step of 0.05 second of the wind field generation. The wind shear was modeled according to the power law with exponent 0.14.

TABLE 5 Mathematical model of faults applied in numerical simulations

Type	Fault Modeling	Consequence
VEF	$\ddot{x}_{vs} + 2\zeta_{vs}\omega_{vs}\dot{x}_{vs} + \omega_{vs}^2 x_{vs} = \omega_{vs}^2 k_u u_{vs} - F_F$	Response delay
VSL	$x_{vs} = x_{vs,\mathrm{VSL}}$	Blade pitch runaway
VWV	$\ddot{x}_{vs} + 2\zeta_{vs}\omega_{vs}\dot{x}_{vs} + \omega_{vs}^2 x_{vs} = \omega_{vs}^2 k_{u,\mathrm{WV}} u_{vs}$	Response delay
VCS	$u_{vs} = u_{\mathrm{VCS}} = 0$	Actuator stuck

Abbreviations: VCS, circuit shortage in the valve; VEF, excessive friction in the valve; VSL, slit lock in the valve; VWV, wrong voltage applied in the valve.

TABLE 6 Load cases based on winds and waves

Load Case	U_w, m/s	Turbulence Model	H_s, m	T_p, s
1	11.2	IEC Class C	3.2	10.0
2	14		3.62	10.30
3	17		4.2	10.50
4	20		4.8	10.80

For irregular waves, the Joint North Sea Wave Project (JONSWAP) wave spectrum was used. The peak period (T_p) and significant wave height (H_s) were decided based on their correlation with wind speed for the Statfjord site in the North Sea.[36] Wind and wave directions are aligned. Six 1-hour simulations with different random seeds are carried out for each load case and fault condition to capture the significant stochastic variation.[8]

4.2 | Fault description

The fault studied here can degrade the control quality and accuracy. In order to identify representative and comparable fault magnitudes, we examine the squared integral error of the blade pitch e_{IEBP} during the response in each simulation:

$$e_{\text{IEBP}} = \int_{TF}^{\tau} (\beta_{\text{actual}}(t) - \beta_C(t))^2 dt. \tag{22}$$

On the basis of the load cases described in Table 6, the fault magnitude has been decided by measuring e_{IEBP}. Figure 10 shows the average e_{IEBP} values for VEF and VWV faults during 400 seconds after fault occurs. The time of fault (TF) is 100 seconds after the turbine reaches the steady-state condition.

For the response study, several different magnitudes M1, M2, and M3 are simulated to illustrate the severity of the faults. The input corresponding to M1, M2, and M3 here has been decided based on the value of e_{IEBP} = 0.006, 0.018, and 0.03 (in fault-free e_{IEBP} = 0.001 432) in VEF and VWV faults, respectively, and is given in Table 7. In case of the VSL fault, both the positive (VSL^+) and negative (VSL^-) stuck valve spool positions have been considered. There is no magnitude in the VCS fault. The fault-free cases correspond to normal operation.

Figure 11 shows the response in terms of the valve spool position and blade pitch angle under four valve faults in the blade pitch system (blade 3). Two faults, VEF and VWV, make the responses of valve position and blade pitch angle slower due to increased friction and gain change, respectively. As shown in Figure 11A, the valve spool cannot move to until the solenoid force is larger than the excessive friction due to sludge in VEF fault. If the solenoid force exceeds the friction, the valve spool moves quickly to follow the control input, and the blade pitch angle increases suddenly in Figure 11B. In this case, the direction change of the valve spool delays the response of the blade pitch system. The VWV fault delays the response due to gain change.

The valve spool position is stuck after occurrence of a VSL fault. However, the valve is still open, and hydraulic fluid flows continuously to the cylinder, making the pitch angle increase. This fault depends on the direction of the valve position. If the valve is stuck in the right position (positive, VSL^+), the blade pitch angle continuously increases to the maximum pitch angle. If it is left (negative, VSL^-), the pitch angle decreases

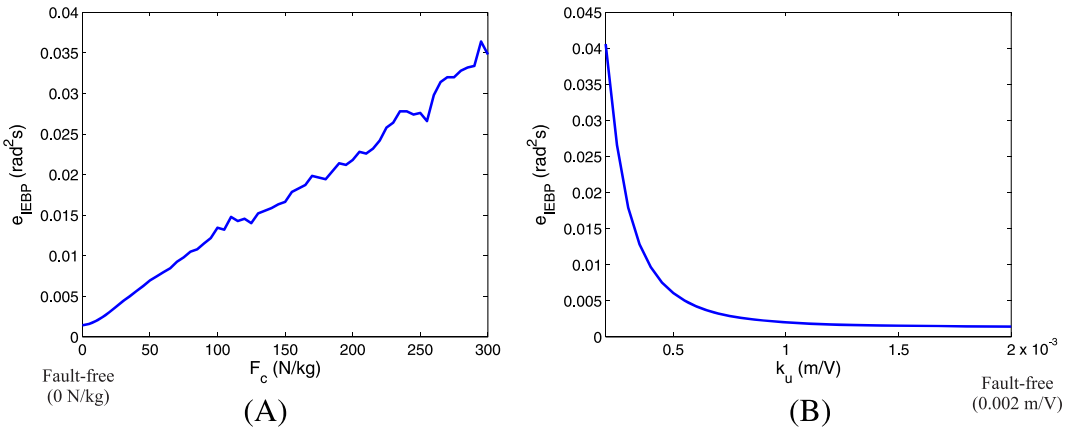

FIGURE 10 Integral error of the blade pitch depends on the fault magnitudes: (A) excessive friction in the valve (VEF) and (B) wrong voltage applied in the valve (VWV) [Colour figure can be viewed at wileyonlinelibrary.com]

TABLE 7 List of magnitudes for VEF and VWV faults

	Magnitude			
Fault Case	**M1**	**M2**	**M3**	**Theoretical Permissible Range**
VEF (F_c), N/kg	45	155	260	<400
VWV (k_u), m/V	0.0005	0.0003	0.000 23	>0

Abbreviations: VEF, excessive friction in the valve; VWV, wrong voltage applied in the valve.

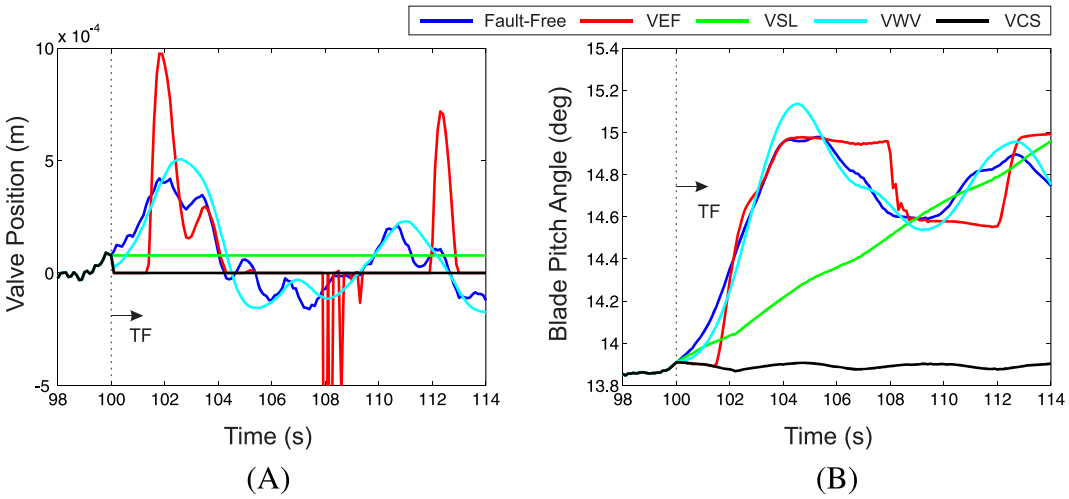

FIGURE 11 Comparison of the valve position and blade pitch angle under fault conditions under LC3: (A) valve position and (B) blade pitch angle. VCS, circuit shortage in the valve; VEF, excessive friction in the valve; VSL, slit lock in the valve; VWV, wrong voltage applied in the valve [Colour figure can be viewed at wileyonlinelibrary.com]

to the minimum pitch angle. When VCS occurs, the input voltage goes to 0 value, and the valve position returns to the neutral position due to the restoring force of the spring. Then, the valve will be closed, and the actuator gets stuck.

4.3 | Wind turbine performances and response analysis

Numerical results for the dynamic responses of the spar-type floating wind turbine under valve faults are presented. The simulations are conducted to evaluate the effect of different fault scenarios. Six realizations of each load case, each lasting for 1 hour, are carried out. The root-mean-square (RMS) values are calculated for the responses for floating wind turbine after fault occurrence (TF is 100 s). The response values are normalized by the corresponding results in the fault-free cases as

$$RV_{\text{norm}} = \frac{RV_i}{RV_{\text{f-free}}} i = 1, 2, 3, 4, \tag{23}$$

where RV_{norm} is the response value normalized by response value in the fault-free case $RV_{\text{f-free}}$ and RV_i is the ith response value (1: VEF, 2: VSL, 3: VWV, and 4: VCS).

4.3.1 | Wind turbine performance

As shown in Figure 12, the blade pitch angle has been influenced by the valve faults in VEF, VWV, and VCS in faulty blade (blade 3). However, these pitch angle differences do not affect the results of rotor speed and power very much.

Figure 13 shows the results of the rotor speed, power, and blade pitch angle under VSL fault. If the valve spool is stuck in the right-side position (VSL^+, positive x_v), hydraulic fluid can flow continuously into the B side of cylinder, and piston moves to the left side of the cylinder until the pressure relief valve starts to work. Due to the difference of blade pitch angle between blades 1 and 3, the rotor speed starts to decrease gradually, which influences power output because of the loss of the generator torque acting on the low-speed shaft described in Figure 13A. Then, the pitch controller adjusts the blade pitch angle of fault-free blades (blades 1 and 2) to 0° to maintain the rated rotor speed, which also increases the aerodynamic thrust. On the other hand, if the valve is locked in the left-side position, the hydraulic fluid can flow to the A side of cylinder. The pitch angle on the faulty blade decreases to 0° due to the piston moving to the right side. In this case, the rotor speed and power output are not influenced significantly by stuck blade 3 as shown in Figure 13B. The aerodynamic torque increases due to the stuck blade (blade 3), and the pitch controller adjusts other two blades (blades 1 and 2) to reduce the aerodynamic torque by increasing their blade pitch angles, thus maintaining the rotor speed.

Figure 14 shows the normalized RMS values of the rotational speed, aerodynamic thrust, and generator power after fault occurrence. VEF, VWV, and VCS faults have little effect on the rotor speed and power production from generator. For VSL fault when the valve spool is stuck at the right position (VSL^+), the generator cannot produce any power because the rotor has been stopped. The blade pitch angle difference (around 20° between blades 1 and 3 in case of VSL^-) causes an increase of aerodynamic thrust as the wind speed increases.

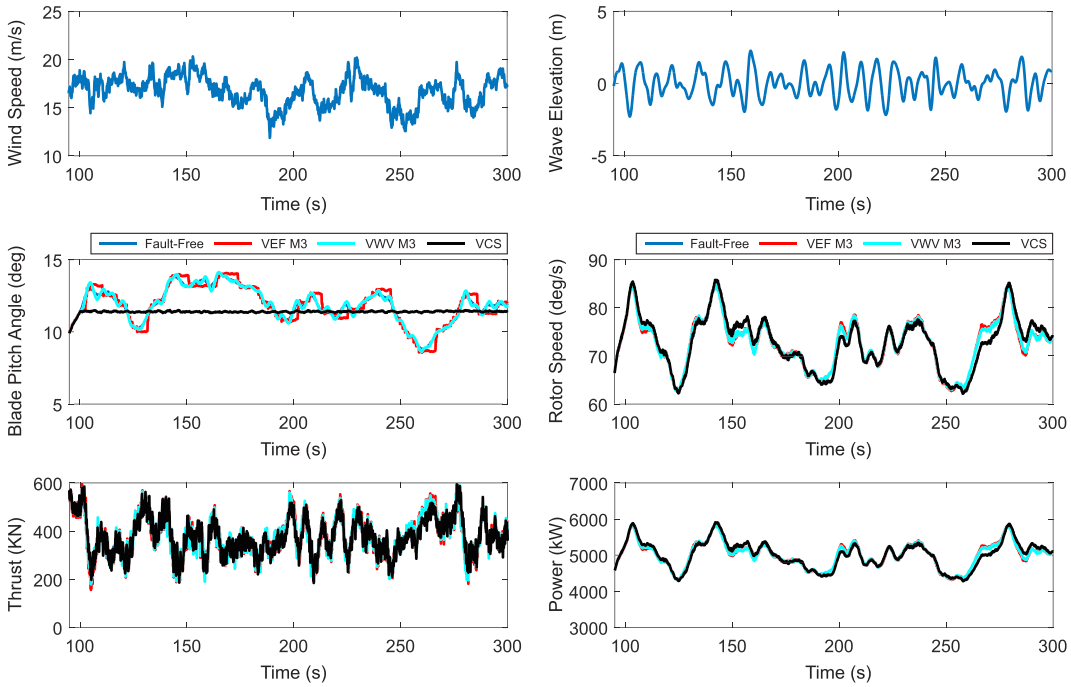

FIGURE 12 Effects of excessive friction in the valve (VEF), wrong voltage applied in the valve (VWV), and circuit shortage in the valve (VCS) faults on wind speed, wave elevation, the blade pitch angle, rotor speed, aerodynamic thrust, and power under LC3 [Colour figure can be viewed at wileyonlinelibrary.com]

4.3.2 | Blade root bending moments

Fault in a pitch actuator affects the torsional, flap-, and edge-wise bending moments in the blade roots. Figure 15 illustrates the load and blade root bending moment directions. Figure 16 shows the effects of fault cases on the RMS of the blade root bending moments, of floating wind turbine. The value in Figure 16 is the difference of RMS values of the blade root bending moment between normal blade (blade 1) and faulty blade (blade 3) along each axis, normalized as follows:

$$\frac{mean\left(RMS\left(M_{\mathrm{BR,fault\text{-}free}}\right)\right) - RMS\left(M_{\mathrm{BR,Blade3}}\right)}{mean\left(RMS\left(M_{\mathrm{BR,fault\text{-}free}}\right)\right)}, \tag{24}$$

where $mean\ (RMS\ (M_{\mathrm{BR,\ fault\text{-}free}})) = (RMS\ (M_{\mathrm{BR,\ Blade1}}) + RMS\ (M_{\mathrm{BR,\ Blade2}}) + RMS\ (M_{\mathrm{BR,\ Blade3}}))/3$ and $RMS\ (M_{\mathrm{BR,\ fault\text{-}free}})$ corresponds to the fault-free condition.

Figure 16 shows that the blade root bending moments due to faults depend on the difference of the blade pitch angle between blades 1 and 3. In fault-free condition, the value of the metric in Figure 16 is nearly 0, implying no rotor imbalance.

In case of VEF faults, the variation of the blade root bending moment along the torsional direction has above 25% of the magnitude of the fault-free blade root bending moments, while the differences in the flap- and edge-wise bending moments are almost 0. VWV has little effect on the blade root bending moment along the torsional, flap-, and edge-wise directions. In VSL^{-}, as the wind speed increases, the difference in flap-wise moments between faulted and fault-free blades can be increased from one to three times. There is also imbalance in the torsion and flap-wise moments for VCS. The imbalance shown here affects the platform motions and tower base bending moments.

4.3.3 | Platform motions and tower base bending moments

The platform motions and tower bending moments are mainly related to wind and wave loads. The spar-type platform has large yaw stiffness from the mooring system. Wave loads do not influence yaw motion much because of the floater's cylindrical shape. Figures 17 and 18 show the effects of fault cases on the RMS of the platform motions and tower base bending moments of floating wind turbine. VEF and VWV faults brought slow response of blade pitch angle. VEF and VWV faults have little effect on platform motions (roll, pitch, and yaw) and tower base bending moments (torsional, fore-aft, and side-side).

The VCS fault tends to cause the actuator to get stuck and leads to aerodynamic imbalance on the rotor plane depending on the operating condition. As a consequence, the yaw and tower torsional moments increase. Yaw motion is increased by approximately 20%, and the torsional

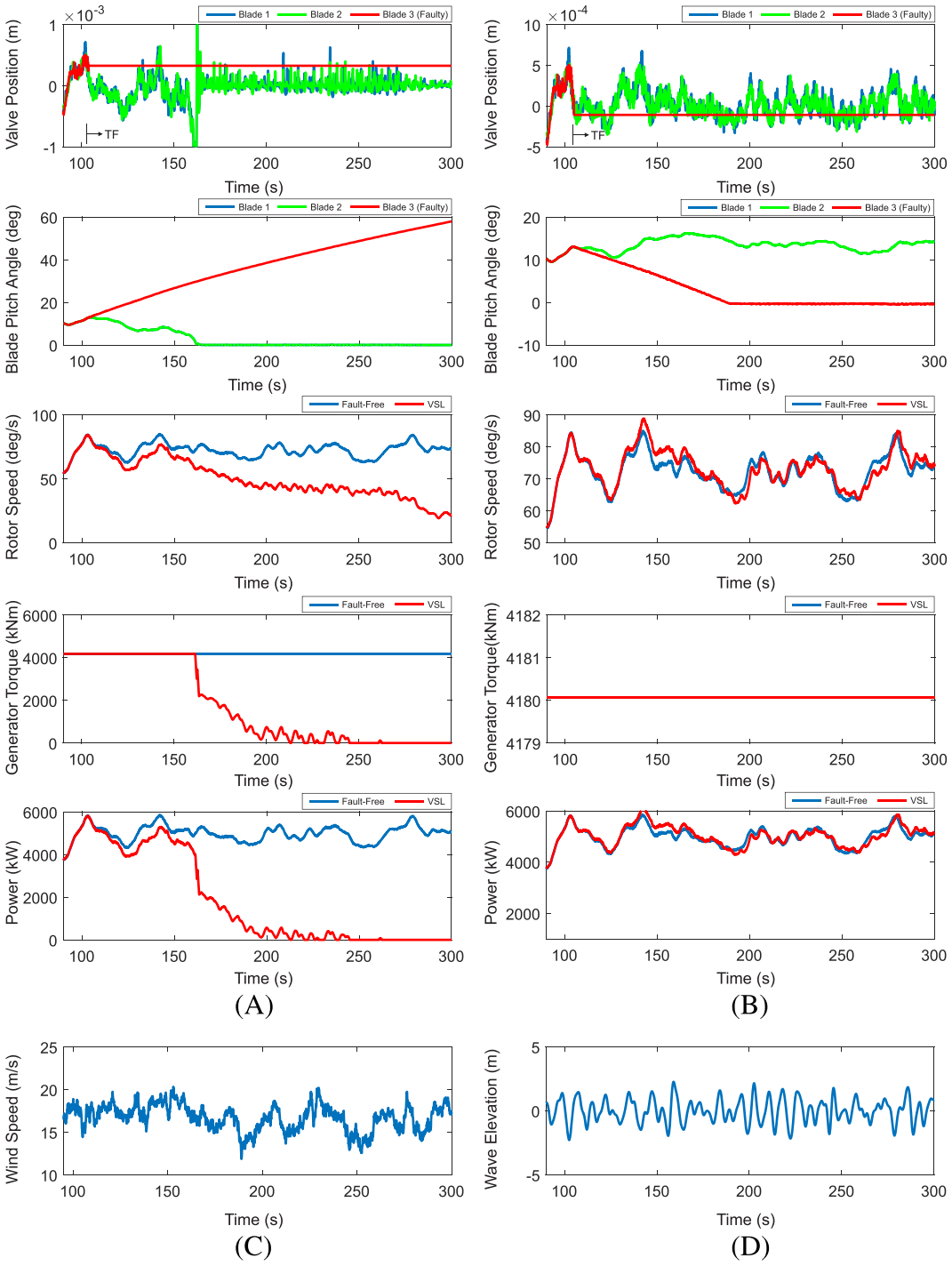

FIGURE 13 Effects of VSL fault on the valve position, blade pitch angle, rotor speed, aerodynamic torque, and power: (A) positive (VSL^{+}) and (B) negative spool position (VSL^{-}) under LC3 with (C) wind speed and (D) wave elevation [Colour figure can be viewed at wileyonlinelibrary.com]

moment can be doubled compared with fault-free conditions. This fault does not greatly affect platform motions (roll and pitch) and tower base bending moments (fore-aft and side-side).

The dynamic responses in case of VSL depend on the spool position. While continuously increasing or decreasing the blade pitch angle in VSL^{+} (positive valve position) or VSL^{-} (negative valve position) faults, increasing blade pitch angle difference causes rotor imbalance. The severe rotor imbalance under VSL fault occurs when the faulty blade is pitched to 0° based on the stuck spool position. The yaw motion is increased by approximately two times, and torsional moment is up to four times larger than the fault-free conditions under VSL^{-} faults. In addition, the increasing aerodynamic thrust as shown in Figure 14B affects platform pitch motion and tower base fore-aft bending moments in Figures 17C and 18C.

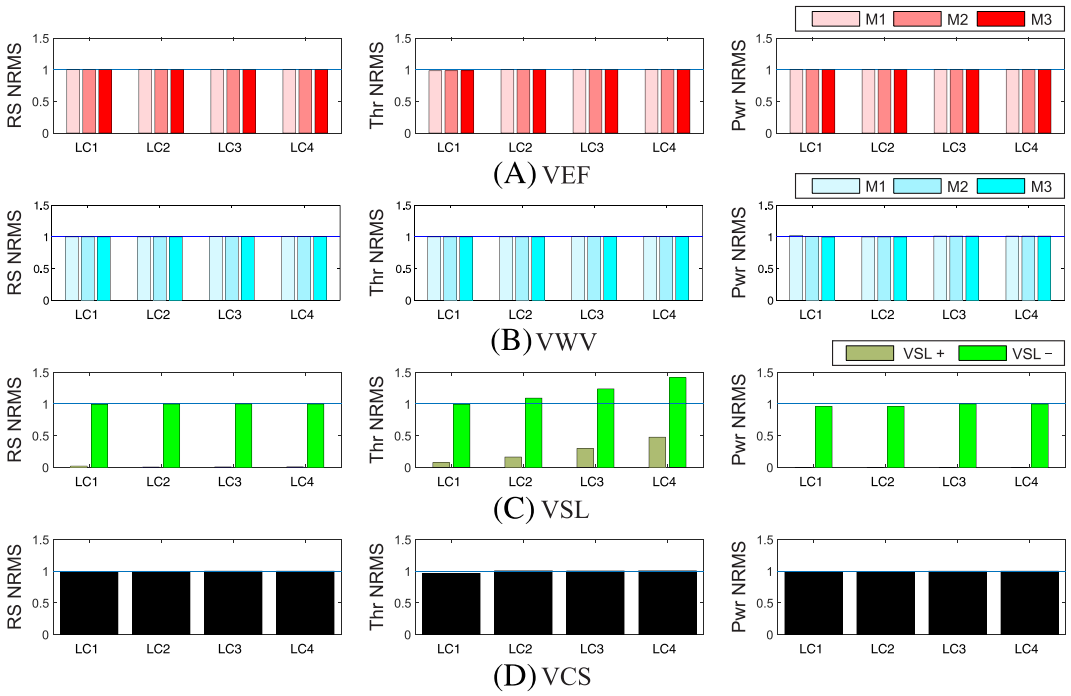

FIGURE 14 Normalized root-mean-square (NRMS) values of the rotor speed, thrust, and power production described by Equation (23) for the floating wind turbine under (A) excessive friction in the valve (VEF), (B) slit lock in the valve (VSL), (C) wrong voltage applied in the valve (VWV), and (D) circuit shortage in the valve (VCS) fault conditions with different fault magnitudes [Colour figure can be viewed at wileyonlinelibrary.com]

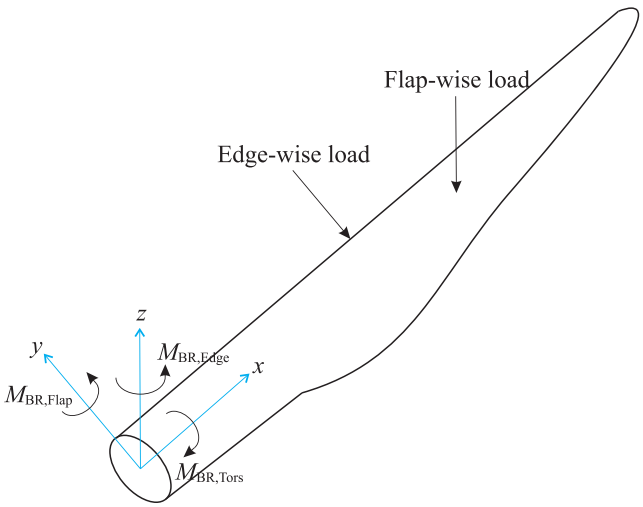

FIGURE 15 The schematic of blade for direction of loads and blade root bending moments [Colour figure can be viewed at wileyonlinelibrary.com]

If the pitch angle difference is beyond a certain limit (above 30°), one or more of the blades acts as a brake, and the rotor speed starts to decrease. With decreasing rotor speed, the wind turbine loses the generator torque acting on the low-speed shaft VSL^{+} fault. The pitch and fore-aft bending moment also decreased. When the faulty blade (blade 3) angle reaches 90°, the rotor has lost much of the aerodynamic thrust, and it affects the results of platform motions and tower base bending moments. The platform motions and tower base bending moments were not affected by the change of the blade root torsional and edge-wise bending moments.

Figure 19 shows a comparison of normalized expected maxima of platform motions and tower base bending moments in above-rated wind speed region. Response values that are platform motions and tower base bending moments are divided by the fault-free values of the expected maxima. These faults have been considered: VEF M3, VSL^{-}, VWV M3, and VSC. Similar to the RMS values shown in Figures 16 and 17, the

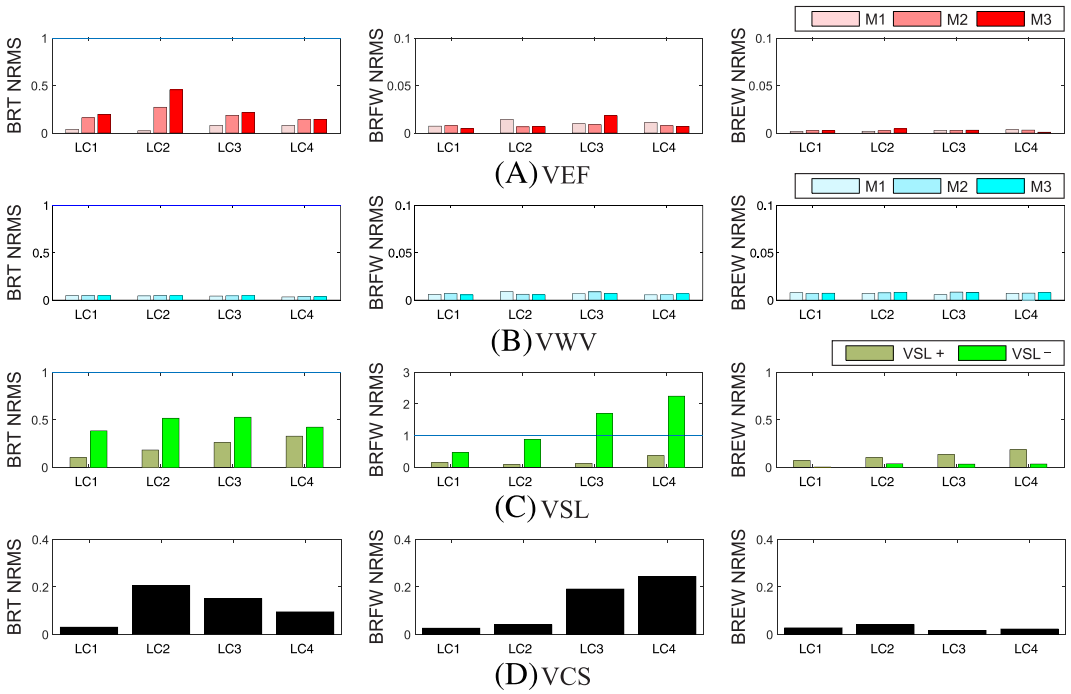

FIGURE 16 Normalized root-mean-square (NRMS) values of the blade root torsional (BRT), blade root flap-wise (BRFW), and blade root edge-wise (BREW) bending moments described by Equation (24) for the floating wind turbine under (A) excessive friction in the valve (VEF), (B) slit lock in the valve (VSL), (C) wrong voltage applied in the valve (VWV), and (D) circuit shortage in the valve (VCS) fault conditions with different fault magnitudes [Colour figure can be viewed at wileyonlinelibrary.com]

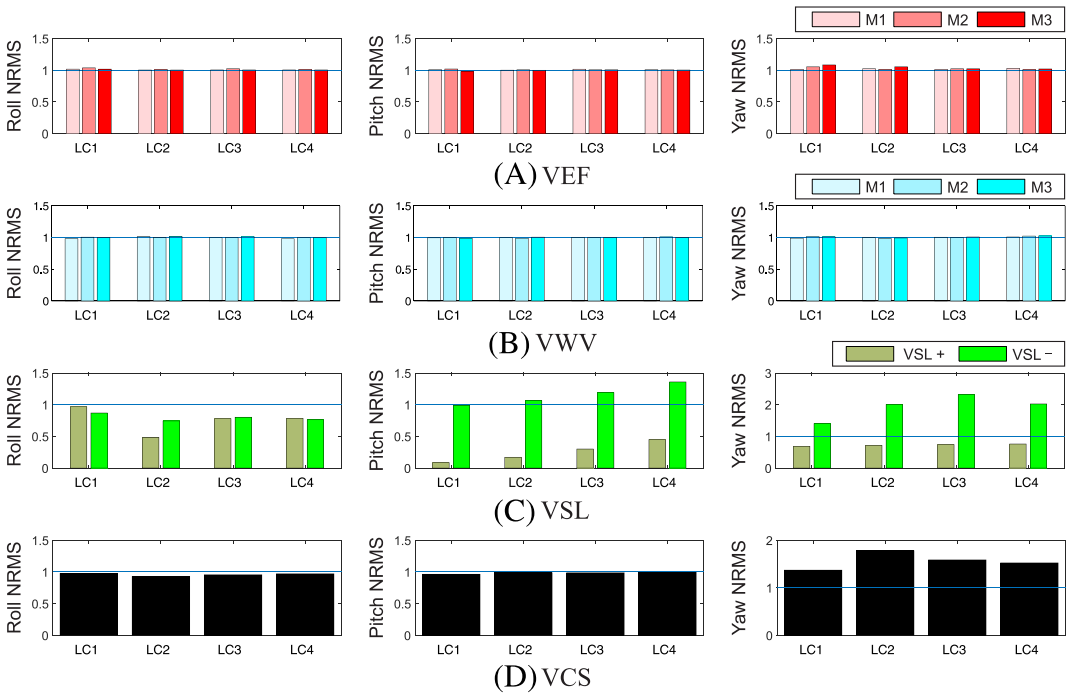

FIGURE 17 Normalized root-mean-square (NRMS) values of the platform roll, pitch, and yaw motions described by Equation (23) for the floating wind turbine under (A) excessive friction in the valve (VEF), (B) slit lock in the valve (VSL), (C) wrong voltage applied in the valve (VWV), and (D) circuit shortage in the valve (VCS) fault conditions with different fault magnitudes [Colour figure can be viewed at wileyonlinelibrary.com]

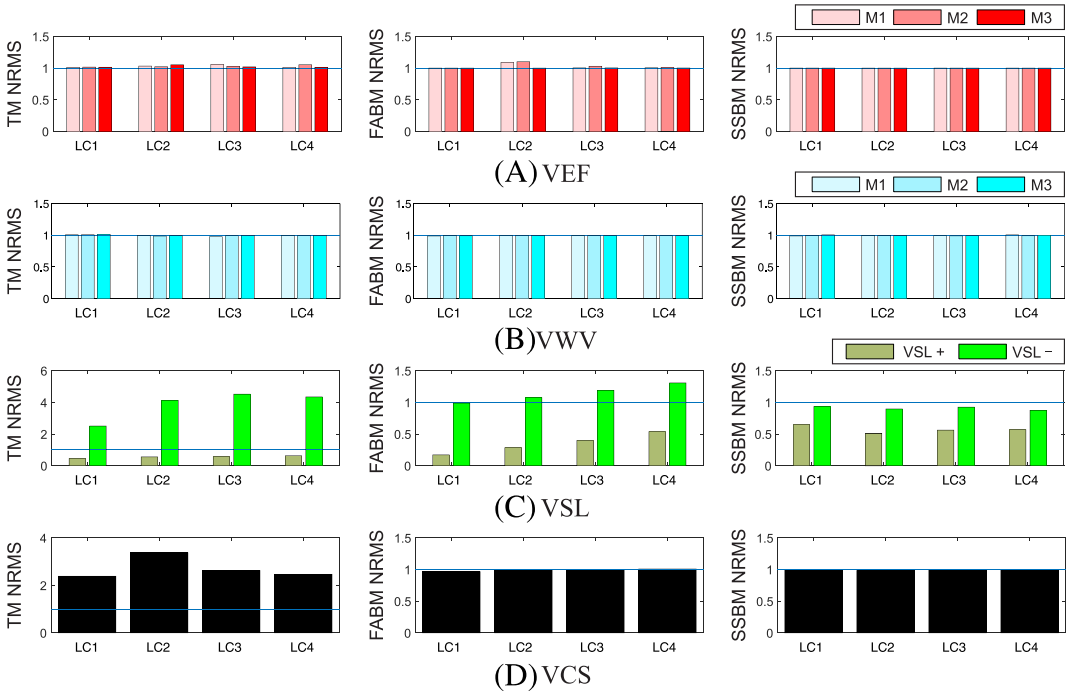

FIGURE 18 Root-mean-square (RMS) values of the torsional moment (TM), fore-aft bending moment (FABM), and side-side bending moment (SSBM) described by Equation (23) for the floating wind turbine under (A) excessive friction in the valve (VEF), (B) slit lock in the valve (VSL), (C) wrong voltage applied in the valve (VWV), and (D) circuit shortage in the valve (VCS) fault conditions with different fault magnitudes [Colour figure can be viewed at wileyonlinelibrary.com]

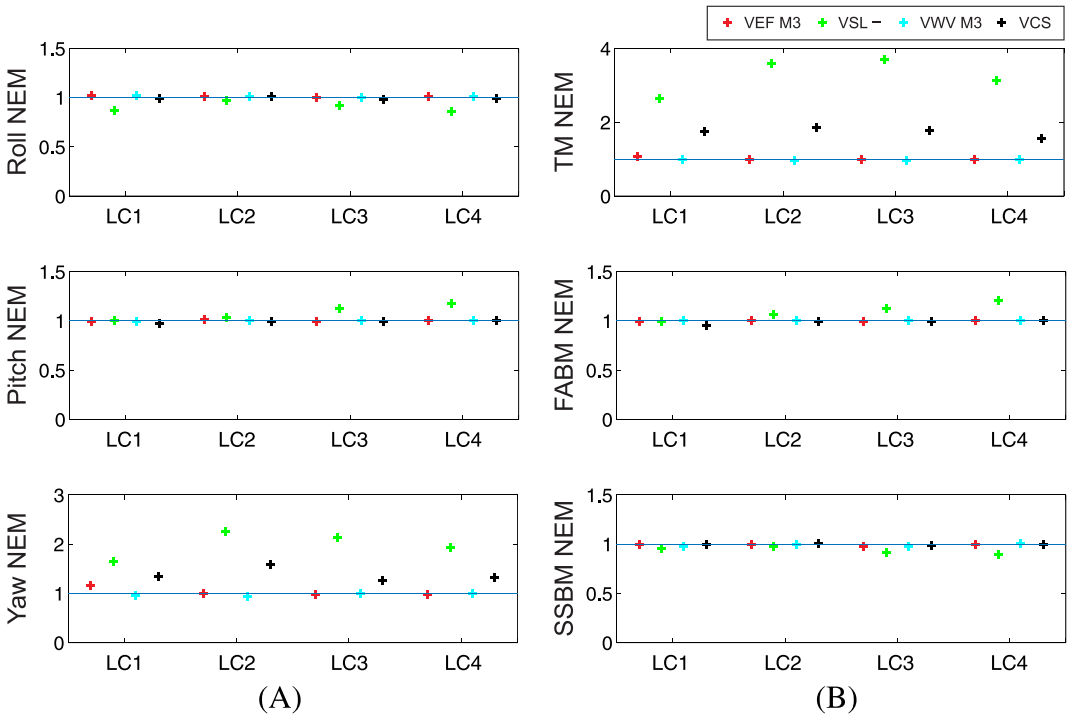

FIGURE 19 Normalized expected maximum (NEM) response values: (A) platform motions and (B) tower base bending moments [Colour figure can be viewed at wileyonlinelibrary.com]

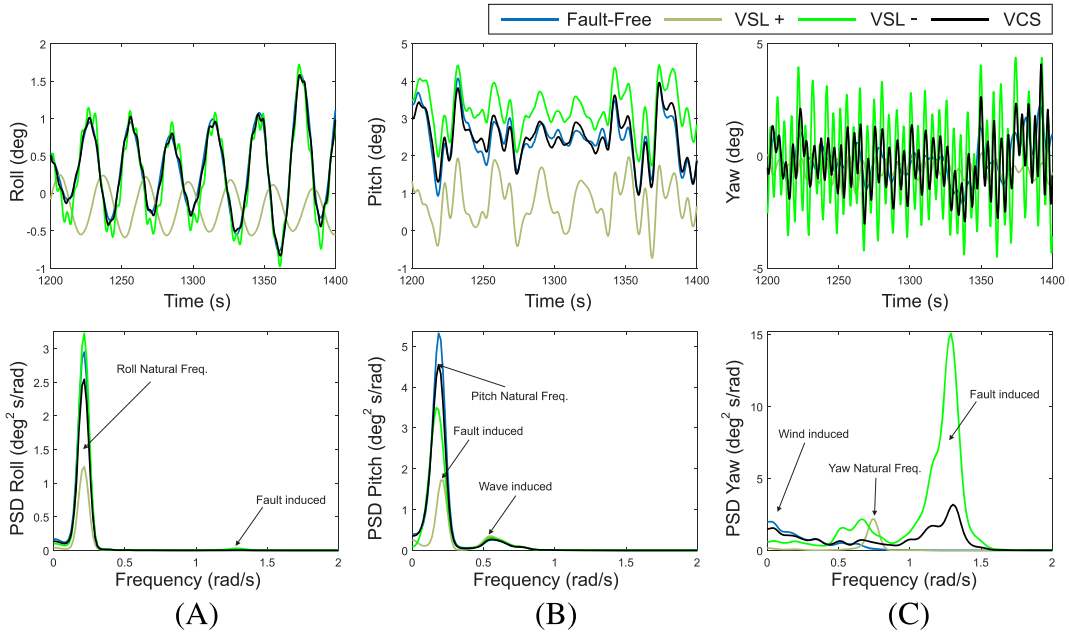

FIGURE 20 Time realization and power spectral density (PSD) of the platform (A) roll, (B) pitch, and (C) yaw motions in LC3 [Colour figure can be viewed at wileyonlinelibrary.com]

platform motions and base bending moments are not sensitive to response delay due to VEF M3 and VWV M3 faults. VSL$^-$ and VSC faults are dominant in yaw and tower base torsional moments.

Figure 20 presents the effects of VSL and VCS faults on the power spectral density (PSD) of the platform roll, pitch, and yaw responses for LC3. The sample duration is 1 hour under faults in stationary condition. The response at the natural frequency in roll motion increases. VSL$^-$ and VCS faults slightly influenced platform pitch motion due to the small blade angle difference. The loss of aerodynamic thrust causes reduced amplitudes and changed frequencies in platform pitch and yaw in VSL$^+$.

The asymmetric force acting on the rotor triggers large aerodynamic excitation of the tower and the spar-type platform. The VSL$^-$ fault has a large effect on the yaw motions compared with the other fault cases in stationary responses. The yaw response is greatly increased, and roll and pitch resonant responses are relatively decreased under the VSL fault when the valve position is negative. In addition, the fault-induced frequency of 1.288 rad/s due to VCS and VSL$^-$ faults corresponds to the 1P frequency of the wind turbine at rated speed.[37]

5 | CONCLUDING REMARKS

This paper deals with numerical modeling and response analysis of the hydraulic pitch actuator in a floating spar-type wind turbine in valve fault conditions. The pitch-regulated NREL 5-MW wind turbine model mounted on the OC3-Hywind floater with three catenary mooring cables has been used in these simulations. Fully coupled time-domain simulations were conducted for the dynamic response analysis using SR with a baseline controller under various environmental conditions with correlated wind and waves. The baseline controller maintained a constant generator torque above the rated wind speed. The hydraulic pitch system was modeled by a pressure supply pump, directional control valve, hydraulic cylinder, and fluid reservoir. The valve spool position is controlled by a PI controller, where a voltage signal is determined from the piston position error that regulates the flows to the two-cylinder sides.

Up to 25% of the hydraulic system's failures are caused by oil contamination with poor filtration. In this paper, two mechanical and two electrical faults have been modeled to check the effect of faults. They include excessive friction (VEF), slit lock (VSL) on spool, wrong voltage applied (VWV), and circuit shortage (VCS) in the directional control valves. This results in sludge buildup on the surface of the spool and bore, which increases the possibility of excessive friction (VEF) or slit lock (VSL). Also, additional current through the solenoid changes its coil impedance and can lead to damages, resulting in the wrong voltage being applied (VWV) and circuit shortage (VCS).

VEF and VWV had minor effects on the floating wind turbine responses compared with the other faults. The faults VCS and VSL lead to an increased aerodynamic thrust due to the difference of the blade pitch angle between fault-free and faulty blade. Serious rotor imbalance occurs while the wind turbine is operating. As a consequence of the rotor imbalance, the platform's yaw and tower torsional moments increase. The VSL$^-$ fault is the most severe fault case regarding platform yaw motion and tower base bending moment. The fault-induced frequency incurring from VSL$^-$ fault is the 1P frequency of the wind turbine. If faults continue, the damage in the wind turbine structure will be amplified. In summary,

the difference of the blade pitch angle causes rotor imbalance, which affects the yaw motion and tower base torsional bending moment. The pitch angle difference also influences the aerodynamic thrust, platform pitch motion, and tower base fore-aft bending moment.

In order to validate the models of fault effects in the wind turbines, field measurements of the blade pitch actuator under faults are needed. In addition, faults affect the wind turbine performance and structural responses of wind turbines. Hence, it is important to detect, diagnose, and mitigate faults at the early stage before they propagate to failure of components.

ACKNOWLEDGEMENTS

This work was supported by the MIT-NTNU-Statoil Wind Turbine Program (project no. 40136503) funded by Equinor (formerly Statoil). The authors gratefully acknowledge the support of Equinor and the Research Council of Norway(Norges Forskningsråd) through the Centre for Ships and Offshore Structures (CeSOS) and Centre for Autonomous Marine Operations and Systems (AMOS) at NTNU for the present study.

ORCID

Seongpil Cho https://orcid.org/0000-0002-6613-4592
Erin E. Bachynski https://orcid.org/0000-0002-1471-8254
Amir R. Nejad https://orcid.org/0000-0003-0391-8696

REFERENCES

1. Ribrant J, Bertling L. Survey of failures in wind power systems with focus on Swedish wind power plants during 1997-2005. In Power Engineering Society General Meeting, 24–28 Jun 2007. IEEE, Energy Conversion. *IEEE Transactions: Stockholm Denmark*. 2007;22:1-8.
2. Gayo J B, Reliability-focused research on optimizing wind energy system design, operation and maintenance: tools, proof of concepts, guidelines & methodologies for a new generation, Final Publishable Summary of Results of Project ReliaWind, 2011.
3. Carroll J, McDonald A, McMillan D. Failure rate, repair time and unscheduled O&M cost analysis of offshore wind turbines. *Wind Energy*. 2016;19:1107-1119. https://doi.org/10.1002/we.1887
4. Tavner P. *Offshore Wind Turbines: Reliability*. London, UK: Availability and Maintenance, The Institution of Engineering and Technology (IET); 2012.
5. Dinwoodie I, McMillan D, Revie M, Lazakis I, Dalgic Y. Development of a combined operational and strategic decision support model for offshore wind. *Energy Procedia*. 2013;35:157-166.
6. Hau E. 2013. Wind Turbines: Fundamentals, Technologies, Application, Economics. Springer Science & Business Media.
7. Wind Nordzee, Operations report 2009, Technical Report OWEZ_R_000_20101112, Nordzee Wind, 2010.
8. Jiang Z, Karimirad M, Moan T. Dynamic response analysis of wind turbines under blade pitch system fault, grid loss, and shutdown events. *Wind Energy*. 2014;17:1385-1409. https://doi.org/10.1002/we.1639
9. Chaaban R, Ginsberg D, Fritzen CP. Structural load analysis of floating wind turbines under blade pitch system faults. *Wind Turbine Control and Monitoring*. 2014;301-334. Springer
10. Bachynski EE, Etemaddar M, Kvittem MI, Luan C, Moan T. Dynamic analysis of floating wind turbines during pitch actuator fault, grid loss, and shutdown. *Energy Procedia*. 2013;35:210-222.
11. Etemaddar M, Blanke M, Gao Z, Moan T. Response analysis and comparison of a spar-type floating offshore wind turbine and an onshore wind turbine under blade pitch controller faults. *Wind Energy*. 2016;19:35-50. https://doi.org/10.1002/we.1819
12. Chiang MH. *A novel pitch control system for a wind turbine driven by a variable-speed pump-controlled hydraulic servo system Mechatronics*. 2011;21:753-761.
13. Lu B, Li Y, Wu X and Yang Z 2009 A review of recent advances in wind turbine condition monitoring and fault diagnosis Proceedings of the 2005 IEEE International Conference on Robotics and Automation ICRA 2005 pp 2290-2295
14. Pros and cons of hydraulic pitch systems, https://www.fsenergy.com/technology/hydraulic-vs-electric-pitch/. Fritz Schur Energy.
15. Hansen MH, Kallesøe BS. *Servo-elastic dynamics of a hydraulic actuator pitching a blade with large deflections*. Journal of Physics: Conference Series; 2007 (Vol. 75, No. 1, p. 012077).
16. Frøyd L, Dahlahug OG. Effect of pitch and safety system design on dimensioning loads for offshore wind turbines during grid fault. *Energy Procedia*. 2012 Jan 1;24:36-43.
17. Rakoto L, Schorsch J, Kinnaert M. Modelling hydraulic pitch actuator for wind turbine simulation under healthy and faulty conditions. *IFAC-PapersOnLine*. 2015 Jan 1;48(21):577-582.
18. Jonkman J, Butterfield S, Musial W, Scott G. Definition of a 5-MW reference wind turbine for offshore system development. *Technical Report NREL/TP-500-38060 USA*. 2009.
19. Jonkman J. *Definition of the floating system for phase IV of OC3* Technical Report NREL/TP-500-47535 *USA*, 2010
20. SINTEF Ocean. Simo 4.15.0 user guide; 2018.
21. SINTEF Ocean. Riflex 4.15.0 user guide; 2018.
22. Larsen TJ, Hanson TD. A method to avoid negative damped low-frequency tower vibration for a floating, pitch controlled wind turbine. *Journal of Physics: Conference Series*. 2007;75:012073.

23. DSTI - Dynamic Sealing Technologies, Inc., How do rotary unions work in wind turbines? *Youtube Video*]. Retrieved from. https://www.youtube.com/watch?v=QvisCF0jWs0
24. Lyons William, Wind Turbine Tour [Youtube Video]. Retrieved from https://www.youtube.com/watch?v=8wK1qmRv_l8
25. Karpenko M, Sepehri N. Fault-tolerant control of a servohydraulic positioning system with crossport leakage. *IEEE Transactions on Control Systems Technology*. 2005 Jan;13(1):155-161.
26. Directional control valves, pilot-operated, with electrical position feedback and integrated electronics (OBS): RE29093, Rexroth, 2016.
27. Merritt HE. Hydraulic Control Systems. *John Wiley & Sons*. 1967.
28. Albers P. Motion Control in Offshore and Dredging. *Springer*. 2010.
29. Šulc B, Jan JA. Non linear modelling and control of hydraulic actuators. *Acta Polytechnica*. 2002;3(3): 41–47.
30. Hydraulic cylinders: 380 bar series-production range. *Liebherr*.
31. Dutton K, Thompson S. *Barraclough B*. Prentice Hall: The Art of Control Engineering; 1997.
32. Cho S, Gao Z, Moan T. Model-based fault detection, fault isolation and fault-tolerant control of a blade pitch system in floating wind turbines. *Renewable Energy*. 2017;120:306-321.
33. Watton J. *Modelling*. Monitoring and Diagnostic Techniques for Fluid Power Systems: Springer; 2007.
34. Jonkman J and Kilcher L. *TurbSim user's guide* Technical Report NREL *USA*, 2012
35. IEC 61400-1: Wind turbines—part 1: design requirements. *International Electrotechnical Commission*. 2005.
36. Hasselmann K, Barnett TP, Bouws E, et al. Measurements of wind-wave growth and swell decay during the Joint North Sea Wave Project (JONSWAP). *Ergänzungsheft*. 1973;8-12.
37. Jonkman JM, Jonkman BJ. Fast modularization framework for wind turbine simulation: full-system linearization. *Journal of Physics: Conference Series*. 2016; 753, 082010.
38. IEC 61400-3: Wind turbines – Part 3 Design requirements for offshore wind turbines. International Electrotechnical Commission. 2005.

How to cite this article: Cho S, Bachynski EE, Nejad AR, Gao Z, Moan T. Numerical modeling of the hydraulic blade pitch actuator in a spar-type floating wind turbine considering fault conditions and their effects on global dynamic responses. *Wind Energy*. 2020;23:370–390. https://doi.org/10.1002/we.2438